Diffusion and segregation model for the annealing of silicon solar cells implanted with phosphorus

F. A. Wolf, A. Martinez-Limia, D. Grote, D. Stichtenoth, and P. Pichler, *Senior Member, IEEE*

***Abstract*—We present a fully calibrated model for the diffusion, segregation and activation of phosphorus for typical annealing conditions of implanted silicon solar cells. In contrast to existing process simulation software, this model allows to quantitatively predict doping profile distributions, and thereby sheet resistances, surface concentrations and junction depths. The model also provides an intuitive understanding of the dependence of these quantities on the parameters of the annealing process.**

I. Introduction

CURRENT studies of implanted n-type Si solar cells for industrial production use P implantation with subsequent annealing for the formation of a back surface field (BSF) as well as to facilitate contact formation [1, 2]. A major open question in this context is whether an efficient process flow can be realized [1], and in particular, whether a B-implanted emitter and a P-implanted BSF can be coannealed. High-dose non-amorphising B implants lead to massive structural defects [3, 4], which can only be annealed with high thermal budgets [4, 1]. By contrast, P implants amorphize and need much lower thermal budgets [1] to anneal implant damage. Due to the fast diffusion of P [5] and the necessity of high surface concentrations for the BSF, they even *require* low thermal budgets. Defining an efficient coanneal process is therefore a non-trivial task that can be optimized with the help of simulation. Simulation of B annealing with current tools [6] is predictive for standard implantation conditions and since recently even for fluorine containing plasma implantation [7]. The situation is very different for P, for which post-implantation annealing has not been as thoroughly investigated due to the lower relevance of P for the formation of ultra shallow junctions, and for which modeling is particularly complicated as both interstitials and vacancies contribute to diffusion. Complementary studies of P diffusion from glasses or spray-on sources [8, 9, 10] provide valuable information but are also not conclusive for post-implantation conditions due to the very different state of intrinsic defects at the onset of the annealing process. For the latter situation, only very few simulation studies have been published [11, 12].

F. A. Wolf was, at the time of this work, with Corporate Research, Robert Bosch GmbH, Robert-Bosch-Platz 1, 70839 Gerlingen-Schillerhöhe, Germany. He now is with LMU Munich.

A. Martinez-Limia is with Corporate Research, Robert Bosch GmbH, Robert-Bosch-Platz 1, 70839 Gerlingen-Schillerhöhe, Germany.

D. Grote and D. Stichtenoth are with SolarWorld Industries Thüringen, Arnstadt, Germany.

P. Pichler is with the Fraunhofer Institute for Integrated Systems and Device Technology, Schottkystrasse 10, 91058 Erlangen, Germany and with the Chair of Electron Devices, University of Erlangen-Nuremberg, Cauerstrasse 6, 91058 Erlangen, Germany.

Manuscript received August 2014, published by IEEE JPV Nov 2014, DOI: 10.1109/JPHOTOV.2014.2362358.

In this paper, we present a model that yields quantitatively correct results for a wide range of experimental conditions, in particular, for solar cell processing conditions. The paper is structured as follows. Sec. II discusses diffusion, Sec. III precipitation and Sec. IV interface segregation. Sec. V compares simulation results with experiment and Sec. VI concludes the paper. The parameters of the model are found in the appendix.

II. Diffusion of phosphorus

As the calibration of the diffusion model for P is highly non-trivial so that even state-of-the-art models yield qualitatively wrong results (see Appendix B), we provide a detailed explanation of the fundamental mechanism of high-concentration P diffusion, as is relevant for solar cell production. This provides one with both a clear strategy and an intuition, of how P diffusion models can be recalibrated to address a particular set of experiments.

We consider the following model for the diffusion of P via P-interstitial (PI) and P-vacancy (PV) pairs [13]:

$$\partial_t C_{\mathrm{P}}^{\mathrm{total}} = \partial_t (C_{\mathrm{P}^+} + C_{\mathrm{PI}} + C_{\mathrm{PV}}) = \sum_{X=\mathrm{I,V}} (-\partial_x J_{\mathrm{P}X}), \quad (1a)$$

$$\partial_t C_{\mathrm{I}}^{\mathrm{total}} = \partial_t (C_{\mathrm{I}} + C_{\mathrm{PI}}) = -\partial_x J_{\mathrm{I}} - \partial_x J_{\mathrm{PI}} - R_{\mathrm{IV}} + R_{\mathrm{Iclus}}, \quad (1b)$$

$$\partial_t C_{\mathrm{V}}^{\mathrm{total}} = \partial_t (C_{\mathrm{V}} + C_{\mathrm{PV}}) = -\partial_x J_{\mathrm{V}} - \partial_x J_{\mathrm{PV}} - R_{\mathrm{IV}}, \quad (1c)$$

Therein, C and C^{total} stand for the individual and total concentrations of quantities identified by the index: phosphorus in any configuration (P), substitutional (active) phosphorus (P^+), isolated self-interstitials (I), vacancies (V), as well as PI and PV pairs. Concentrations depend on position x (depth in the Si wafer) and time t. $J_{\mathrm{P}X}$ denotes the currents of the PX pairs (X=I,V) and J_X the currents of the isolated point defects. The reaction of Is with I-clusters is contained in R_{Iclus}, for which we assume the model of [14]. The implementation of the recombination rate R_{IV} for Is with Vs follows Ref. [13]. R_{Iclus} and R_{IV} are not relevant for the following discussion.

The reduced model of Eq. (1), which is the basis for all what follows, assumes the pairing reaction of P with point defects to be in equilibrium. This results in a simple product relation [15] for the concentration of pairs $C_{\mathrm{P}^+X^z} = k_{\mathrm{P}^+X^z} C_{\mathrm{P}^+} C_{X^z}$, where z denotes the charge state of the point defect that binds to phosphorus [16]. Due to the product relation, the currents $J_{\mathrm{P}X}$ in Eq. (1) can be expressed in terms of contributions from the substitutional dopant atoms C_{P^+} and the respective intrinsic point defects C_{X^z} in the pair. Defining the total currents $J_{\mathrm{P}X}$ and J_X as the sum over all charge states, $J_{\mathrm{P}X} = \sum_z J_{\mathrm{P}^+X^z}$ and $J_X = \sum_z J_{X^z}$, it remains to specify the contributions to

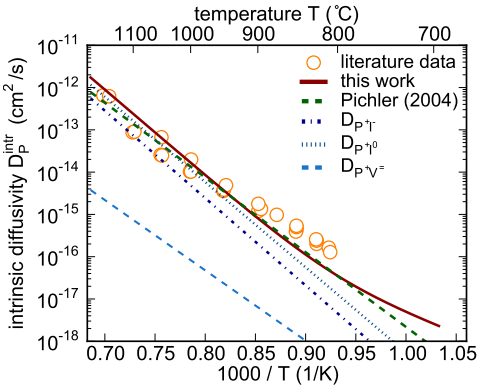

Fig. 1. Intrinsic diffusivity $D_{\mathrm{P}}^{\mathrm{intr}}$ of P. Symbols depict literature data[19, 20, 21, 22] taken from the compilation of [5, p. 320]. The solid line corresponds to the value of $D_{\mathrm{P}}^{\mathrm{intr}}$ obtained for our parameters for $D_{\mathrm{P+I^0}}$, $D_{\mathrm{P+I^-}}$, $D_{\mathrm{P+V^=}}$, which are specified in Appendix A. The contributions from $\mathrm{P^+V^-}$ and $\mathrm{P^+V^0}$ pairs can be neglected and therefore are omitted. For comparison, we plot the fit obtained by [5] described by $1.03e^{-3.507\,\mathrm{eV}/kT}$.

each charge state

$$J_{\mathrm{P}+X^z} = -D_{\mathrm{P}+X^z}\left(\frac{n}{n_i}\right)^{-z}\left(\frac{C_{\mathrm{P}^+}}{C^*_{X^0}}\partial_x C_{X^0} + \alpha_f \frac{C_{X^0}}{C^*_{X^0}}\partial_x C_{\mathrm{P}^+}\right), \tag{2a}$$

$$J_{X^z} = -D_{X^z}\left(\frac{n}{n_i}\right)^{-z}\partial_x C_{X^0}, \tag{2b}$$

where the *field enhancement factor* [17] α_f is

$$\alpha_f = (1 + C_{\mathrm{P}^+}(C^2_{\mathrm{P}^+} + 4n_i^2)^{-\frac{1}{2}}), \tag{3}$$

with n denoting the electron concentration and n_i the intrinsic concentration of charge carriers. $C^*_{X^0}$ stands for the equilibrium concentration of point defect X in charge state $z = 0$, and D_{X^z} and $D_{\mathrm{P}+X^z}$ denote the diffusion constants of the charged intrinsic point defects X and charged PX pairs. Values for D_{X^z} have been well-studied experimentally [18] and we simply assume the default values of Sentaurus Process [6] for them. Values for $D_{\mathrm{P}+X^z}$, by contrast, show a considerable spread over the literature [5], and we discuss their calibration in the following.

a) Low-concentration diffusion: The concentration of intrinsic point defects in the bulk is determined by the interplay of two complementary processes: P diffusion transports intrinsic point defects X via the mobile PX pairs into the bulk while the transport back to the surface goes via self-diffusion of X. At low P concentrations, the former process is negligible in comparison to the latter. P diffusion then causes only insignificant deviations of the concentrations of intrinsic point defects from equilibrium so that the gradients $\partial_x C_{X^0} = 0$ vanish. In this approximation, summing over the charge states of PI and PV pairs as defined in Eq. (2), one obtains a single effective diffusion equation

$$\partial_t C_{\mathrm{P}}^{\mathrm{total}} = \partial_x \sum_{X,z}\left(\alpha_f D_{\mathrm{P}+X^z}\left(\frac{n}{n_i}\right)^{-z}\frac{C_X}{C^*_X}\right)\partial_x C_{\mathrm{P}^+}, \tag{4}$$

which for intrinsic conditions, where $n = n_i$ and $\alpha_f \simeq 1$, gives

$$\partial_t C_{\mathrm{P}}^{\mathrm{total}} = \left(D_{\mathrm{PI}}^{\mathrm{intr}}\frac{C_{\mathrm{I}}}{C^*_{\mathrm{I}}} + D_{\mathrm{PV}}^{\mathrm{intr}}\frac{C_{\mathrm{V}}}{C^*_{\mathrm{V}}}\right)\partial_x^2 C_{\mathrm{P}^+}. \tag{5}$$

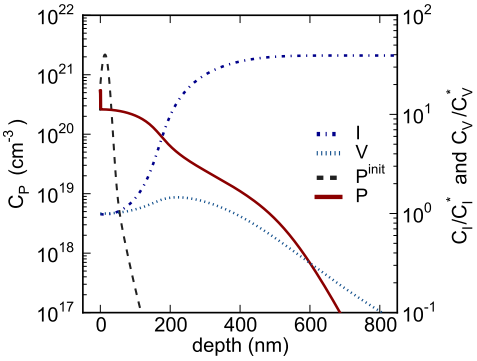

Fig. 2. Details of P diffusion after an implant of $4.5{\cdot}10^{15}\,\mathrm{cm}^{-2}$ at 10 keV annealed at 900 °C for 34 min. The concentration of Is increases when going deeper into the bulk, while the inverse is true for Vs. Note that $C_X/C^*_X = C_{X^0}/C^*_{X^0}$. A similar figure has been shown in Ref. [23].

where we defined the intrinsic diffusion coefficients

$$D_{\mathrm{P}X}^{\mathrm{intr}} = \sum_z D_{\mathrm{P}+X^z}. \tag{6}$$

In this work, we assume that P diffusion is mediated by $\mathrm{P^+I^-}$, $\mathrm{P^+I^0}$, $\mathrm{P^+V^=}$, $\mathrm{P^+V^-}$ and $\mathrm{P^+V^0}$ pairs, as is assumed in Ref. [6]. Fig. 1 compares our calibration for $D_{\mathrm{P+I^0}}$, $D_{\mathrm{P+I^-}}$, $D_{\mathrm{P+V^=}}$ and the resulting value for $D_{\mathrm{P}}^{\mathrm{intr}}$ with experimental data. The parameters $D_{\mathrm{P+I^0}}$, $D_{\mathrm{P+I^-}}$, $D_{\mathrm{P+V^=}}$ can be found in Appendix A. We do not show the parameters $D_{\mathrm{P+V^-}}$ and $D_{\mathrm{P+V^0}}$, which we leave as in the calibration of [6] where they only contribute for temperatures clearly below 800 °C, which is outside the temperature range we are interested in. As seen in Fig. 1, our choice of parameters yields an intrinsic diffusion coefficient close to the fit of Ref. [5], obtained by fitting many experimental results.

b) High-concentration diffusion — kink concentration: For high-concentration diffusion, the diffusion of P has a strong influence on the intrinsic point defect concentrations in the bulk [23, 24]. This leads to strongly inhomogeneous intrinsic point defect distributions and the gradient $\partial_x C_{X^0}$ in the PX current (2a) can no longer be neglected. To understand the physical mechanism that leads to this contribution, consider the typical example shown in Fig. 2. The figure allows to qualitatively interpret the terms in the coupled diffusion equations (1b) by realizing that currents are, via the gradients in Eq. (2), proportional to the slope of the concentration profiles shown in Fig. 2: Clearly, J_{PI} transports Is deeper into the bulk, while J_{I} transports Is back to the surface. The qualitative behavior of J_{V}, by contrast, is not as clearly defined, as the concentration profile for Vs is quite flat for the parameter regime shown in Fig. 2. Generally, comparing the current contributions $J_{\mathrm{P}X}$ with J_X, one observes that $J_{\mathrm{P}X}$ in Eq. (2a) grows strongly w.r.t. C_{P^+}, while J_X in Eq. (2b) does not. For high values of C_{P}, $J_{\mathrm{P}X}$ therefore dominates over J_X, and high amounts of Is are transported into the bulk, whereas close to the surface, the I concentration is still around its equilibrium value (see right ordinate of Fig. 2). This implies (compare (5)) a high effective P diffusion coefficient deeper in the bulk, and a normal P diffusion coefficient close to the surface. This separates two regions in which P diffusion occurs

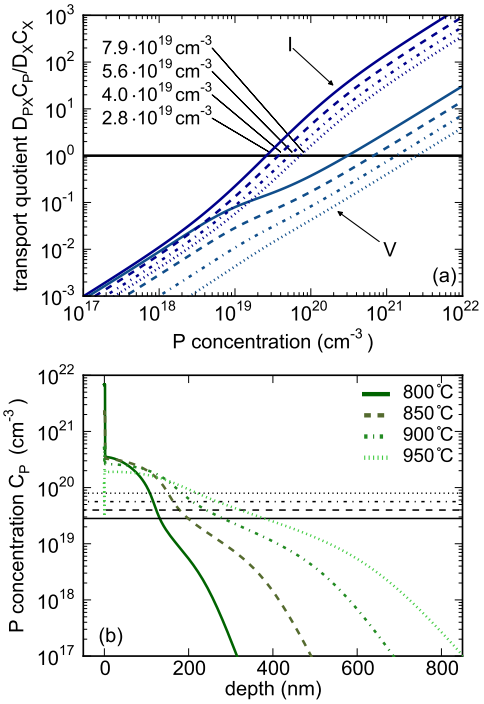

Fig. 3. Panel (a): The contribution of P to I diffusion increases much faster than the one for V diffusion. The estimates for the kink concentration $C_{\mathrm{P}}^{\mathrm{kink,estim}}$ are given by the positions of the intersection of the transport quotient for Is with an ordinate value of unity, as defined in Eq. (9). The numerical values of these estimates are shown for four different temperatures. The legend for the temperatures is given in panel (b). Panel (b): Comparison of the estimate for the kink concentration with a simulation for a P dose of $1{\cdot}10^{15}\,\mathrm{cm}^{-2}$ implanted at 10 keV (see also experimental data in the last section).

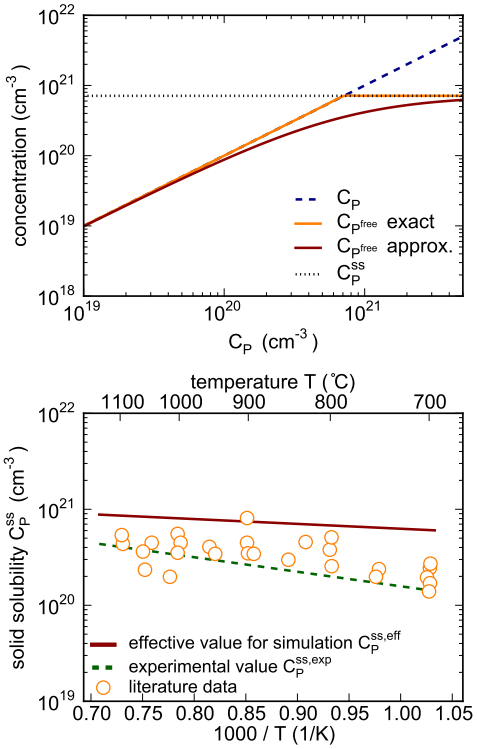

Fig. 4. Equilibrium P activation model. Upper panel: The free (active) P concentration $C_{\mathrm{P}}^{\mathrm{free}}$ is obtained from the total P concentration C_{P} via Eq. (11). The exact value for C_{Pfree} is obtained by usage of Eq. (10) and the approximated value by usage of Eq. (11) for the plateau annealing temperature. The temperature used for the panel is 850 °C. Lower panel: Solubility $C_{\mathrm{P}}^{\mathrm{ss}}$ of electrically active P. The literature data is taken from the compilation of [5] and shows measurements of [25], [26], [27], [28] and [29].

at qualitatively different strengths, which leads to the typical kink in high-concentration P diffusion profiles.

The value of the kink concentration can be estimated with the following argument. The ratio of the currents of X that diffuse via PX and the the currents of X that diffuse isolated equals the ratio of their respective transport capacities [5, Sec. 3.4.7]

$$\frac{D_{\mathrm{P}X}C_{\mathrm{P}+}}{D_X C_X^*} \tag{7}$$

where the effective diffusion coefficients of PX pairs has been introduced as

$$D_{\mathrm{P}X} = \sum_z D_{\mathrm{P}+X^z}\left(\frac{n}{n_i}\right)^{-z}. \tag{8}$$

The kink concentration, i.e. the P concentration at which the two qualitatively different diffusion regions are separated, roughly appears when the transport capacity of the PX pair becomes higher than the transport capacity of the isolated X.

The ratios of transport capacities (7) are shown in their dependences on the P concentration in Fig. 3(a) for our calibrated parameters of Appendix A. The transitions from the domination of self-diffusion to the domination of impurity-atom diffusion are given by intersections of the ratios of the transport capacities with the constant line at an ordinate value of unity. These intersections occur for typical P concentrations as observed in Fig. 2 in the case of I. In the case of V, these intersections occur for so high P concentrations, that their effect can usually not be observed. It is therefore the case of Is, for which the intersection yields an approximation for the appearance of the typical kink,

$$C_{\mathrm{P}}^{\mathrm{kink,estim}} \qquad \text{defined by} \qquad \frac{D_{\mathrm{PI}}C_{\mathrm{P}}^{\mathrm{kink,estim}}}{D_{\mathrm{I}}C_{\mathrm{I}}^*} = 1, \tag{9}$$

where it should be remembered that D_{PI} and D_{I} depend on C_{P} via $\frac{n}{n_i}$. Isolation of $C_{\mathrm{P}}^{\mathrm{kink,estim}}$ in Eq. (9) is therefore tedious. The values for Eq. (9), as obtained for our parameters, are explicitly shown for Is in Fig. 3(a). In Fig. 3(b) we plot these values as horizontal lines together with the simulated P concentration profiles. Agreement is good even on a quantitative level, only for the lowest temperature, it is poorer. Such an analysis provides a systematic strategy to narrow down the calibration of diffusion constants to a small regime that is compatible with a comparison of own experimental data of kink concentrations.

III. Clustering and Precipitation

The active P concentration in P profiles is in the literature found to be best characterized as a plateau, which extends rather deeply into the wafer [see e.g. 10, 30]. Current models [31] implement a dynamical clustering reaction to describe insufficient activation, which leads to results that contradict this experimental evidence: the concentration profile of a

dynamically modeled cluster reduces the active concentration only up to the shallow depth of the as-implanted profile, as the modeled clusters remain immobile throughout the anneailng process. By contrast, with the equally well-established steady-state clustering model, we can directly reproduce the plateau shape. The steady-state model defines a solubility for active P that obeys an equilibrium relation: The fraction of P below this solubility is assumed active and participates in diffusion, the fraction above this solubility is assumed inactive and does not participate in diffusion. In practice, in the diffusion equations of Sec. II, where substitutional P appeared as C_{P^+}, we now replace it with the concentration of free phosphorus C_{Pfree}, obtained from some total P concentration C_{P}.

Taking the solubility model literally, one would define the relationship between C_{Pfree} and C_{P} rigidly in the form

$$C_{\mathrm{Pfree}} \quad \simeq \quad \begin{cases} C_{\mathrm{P}}^{\mathrm{ss}} & \text{for} \quad C_{\mathrm{P}} \geq C_{\mathrm{P}}^{\mathrm{ss}}, \\ C_{\mathrm{P}} & \text{for} \quad C_{\mathrm{P}} \leq C_{\mathrm{P}}^{\mathrm{ss}}. \end{cases} \tag{10}$$

However, this function is not smooth and was found to lead to non-converging numerical solutions. Instead, we use the approximation

$$C_{\mathrm{P}}^{\mathrm{free}} = \frac{C_{\mathrm{P}}^{\mathrm{ss}} C_{\mathrm{P}}}{C_{\mathrm{P}}^{\mathrm{ss}} + C_{\mathrm{P}}} \tag{11}$$

which corresponds to the activation model *Solid* of Sentaurus Process [6].

In the upper panel of Fig. 4, we show the approximation of the free P concentration together with the rigid formulation (10). One observes a significant mismatch for the region around $C_{\mathrm{P}} = C_{\mathrm{P}^+}^{\mathrm{ss}}$. The solid solubility as used with the approximate expression (11) has thus to be considered an effective parameter, employed to satisfy the necessity to use a smooth functional dependence of $C_{\mathrm{P}}^{\mathrm{free}}$ on C_{P}. Therefore, to calculate the sheet resistance after the simulation, we employ the rigid relation, fitted to well-checked experimental values as shown in the lower panel of Fig. 4, and evaluated for the plateau annealing temperature.

IV. Interface segregation of phosphorus

In the case of interface segregation, current models [31] qualitatively overestimate segregation for the experimental conditions studied here. In particular, they do not show a reversible segregation [32] that should occur for the high temperatures used in typical solar cell processing conditions: After ion implantation, the high amount of implantation-induced Is leads to *transient enhanced diffusion* already at low temperatures, where the energy-driven segregation is much stronger than at high temperatures, where entropy-driven redistribution usually becomes so strong that the segregated P is again released from the interface traps.

Models for the dynamic segregation of P at the SiO_2/Si interface approximate the interface as an infinitely thin layer [33, 34]. The traps in this layer can in principle dynamically capture and release P to both sides of the interface. This model is described by the fluxes in (J^t) and out (J^e) of the interface, leading to the following time evolution equation for the number of trapped P atoms N_{P} [35, 6]

$$\partial_t N_{\mathrm{P}} = J^t - J^e \tag{12}$$

$$J^t = k_t (N_t - N_{\mathrm{P}}) C_{\mathrm{P}^+} \tag{13}$$

$$J^e = k_e N_{\mathrm{P}} (C_{\mathrm{P}}^{\mathrm{ss,seg}} - C_{\mathrm{P}^+}) \tag{14}$$

Here, $C_{\mathrm{P}^+} \equiv C_{\mathrm{P}^+}(x)|_{x=0}$ is the P concentration on the silicon side of the interface that is situated at $x = 0$. $C_{\mathrm{P}}^{\mathrm{ss,seg}}$ is a limiting concentration in the bulk, usually at least the solid solubility, and k_t and k_e are trapping and emission rates. In general, the interface can exchange dopants with both neighboring materials, and one has a sum in Eq. (12) that reads $\partial_t N_{\mathrm{P}} = \sum_{a=\mathrm{Si,SiO_2}} J_a^t - J_a^e$. In practice, almost no dopant is exchanged with the oxide side [31]: $J_{\mathrm{Ox}}^t \simeq 0$ and $J_{\mathrm{Ox}}^e \simeq 0$. With this we can keep the simple notation of Eq. (12) and do not have to account for the material-dependent terms.

In equilibrium, Eq. (12) yields

$$\frac{N_{\mathrm{P}}}{N_t - N_{\mathrm{P}}} = \frac{C_{\mathrm{P}^+}}{C_{\mathrm{P}}^{\mathrm{ss,seg}} - C_{\mathrm{P}^+}} \frac{k_t}{k_e}, \tag{15}$$

which implies that $\frac{k_t}{k_e}$ can be associated with a segregation free energy ΔG,

$$\frac{k_t}{k_e} = e^{\Delta G / kT}. \tag{16}$$

One must have $\Delta G > 0$ to observe segregation of P for sufficiently low temperatures. From this one concludes that, if k_t and k_e both follow Arrhenius laws, the activation energy of k_e must be higher than that of k_t, which is a rigorous constraint for these parameters. We finally note that interface segregation has a major influence on the surface concentration, which determines contact properties as well as charge carrier recombination at the surface.

V. Experimental validation

We compare the simulation results of our model with typical solar cell processing experiments in Figs. 5 and 6, and find good agreement in all cases, which vary over a wide range of temperatures and implantation doses. While the high-temperature conditions of Fig. 6 do not pose a difficult case, for the lower temperature conditions of Fig. 5, the interplay of transient enhanced diffusion, segregation and activation phenomena has to be correctly captured by the model, in order to reproduce the typical benchmarks of kink position, junction depth and surface concentration.

A prominent feature in the experimental profiles are the peaks at the SiO_2/Si interface, which are signatures of inactive interface-segregated P atoms. As already mentioned at the beginning of Sec. IV, interface segregation is reversible and can therefore be strongly influenced by the detailed annealing protocol. We show the time evolution of the segregated P dose in Fig. 7(a), where for the lowest temperature, the segregated dose increases during the whole annealing process. For higher temperatures, the dose is partly recovered, i.e. it reenters the bulk when reaching the plateau annealing temperature. Only at the end of the annealing process, during the low temperatures that occur during ramp-down, the segregated dose increases again. This increase of the segregated dose

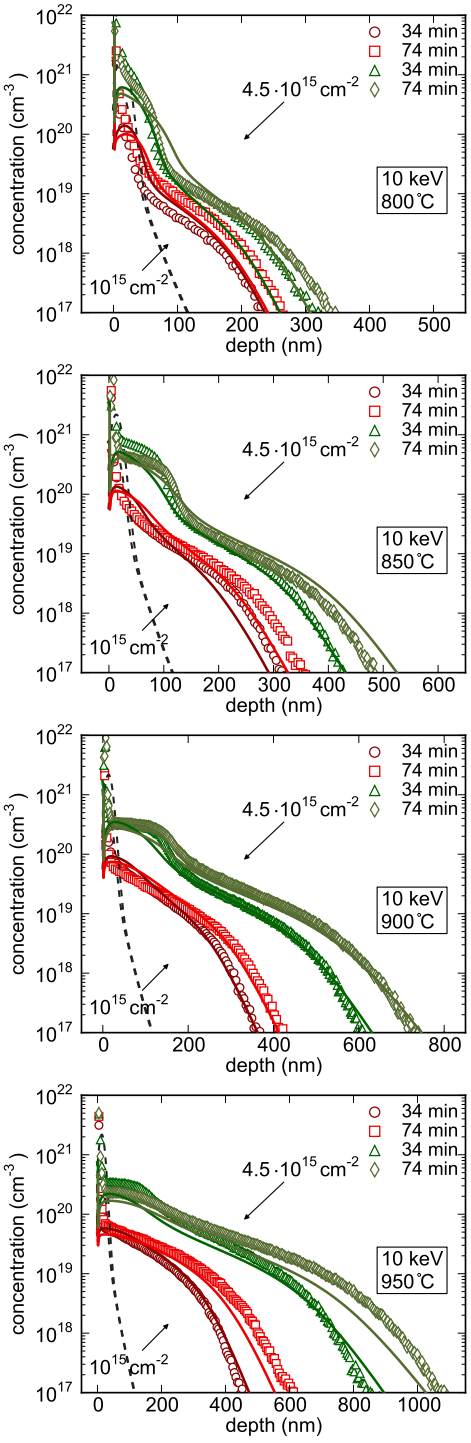

Fig. 5. P concentration profiles for annealing of implanted Phosphorus at 10 keV and doses of $1{\cdot}10^{15}\,\mathrm{cm}^{-2}$ and $4.5{\cdot}10^{15}\,\mathrm{cm}^{-2}$. Symbols depict experimental results obtained at Bosch Solar Energy, lines depict simulation results. The annealing temperatures and times are given in the panels. Heating and cooling ramps proceed at 10 K/min, starting at 600 °C. The interface to the oxide is at 0 μm. Simulations performed using the calibrated model described in Sec. A.

during ramp down can degrade the quality of the back surface field, as it considerably reduces the P surface concentration.

Finally, in Fig. 8, we show experimental and simulation results for the sheet resistances obtained for the dopant profiles shown in Fig. 5. We find very good agreement using the

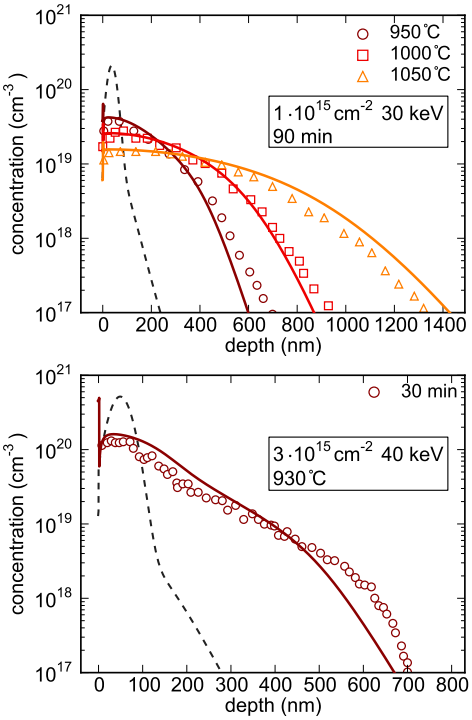

Fig. 6. P concentration profiles after implantation and annealing. Parameters are given in the figure. Experimental data from [36] (upper panel) and [37] (lower panel). Simulations performed using the calibrated model described in Sec. A.

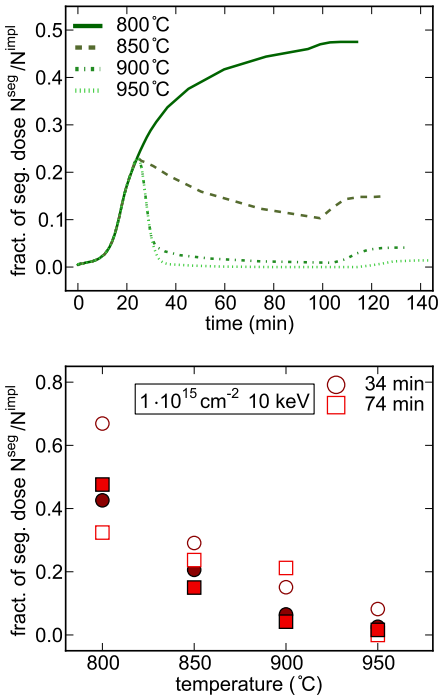

Fig. 7. The segregated P dose for the concentration profiles of the $1{\cdot}10^{15}\,\mathrm{cm}^{-2}$ dose in Fig. 5. Upper panel: Simulated time evolution. Lower panel: Comparison with experiment. Lines and filled symbols depict the simulation, open symbols the experiment. The ramp up and down proceeded with 10 K/min, starting and ending at 600 °C. 800 °C are therefore reached after 20 min of annealing. Up to this time and slightly longer, all curves agree.

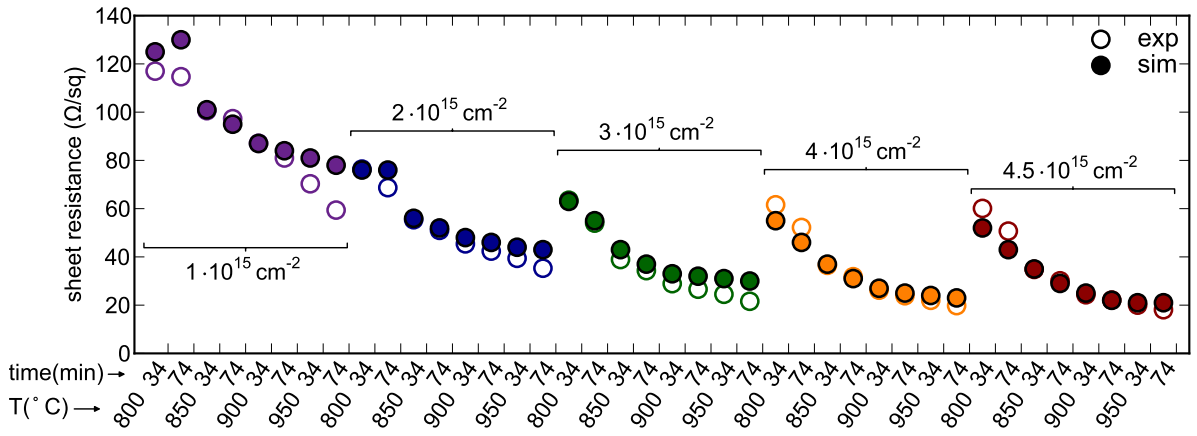

Fig. 8. Sheet resistance measurements compared to values calculated from simulated profiles, using the the mobility values of Sentaurus Process [6]. The corresponding concentration profiles for the cases with P doses of $1{\cdot}10^{15}\,\mathrm{cm}^{-2}$ and $4.5{\cdot}10^{15}\,\mathrm{cm}^{-2}$ have been shown in Fig. 5.

method explained in Sec. III. Again, we find the signature of segregation: the values of R_s for the 800 °C data points are significantly higher than the values of R_s obtained for higher temperatures, separated by a step that can be associated with the irreversible segregation at 800 °C and the reversible segregation for higher temperatures (Fig. 7(a)). The non-trivial activation phenomena can therefore be explained with segregation, whereas the influence of precipitation is easy to understand: precipitation only contributes for very high P concentrations and shows a very weak and smooth temperature dependence as shown in Fig. 4.

VI. Conclusion

We presented a predictive model for the diffusion and segregation of P in Si for typical solar cell processing conditions. We clarified important physical mechanisms and their relation to profile form and sheet resistance. The presented model is suitable to optimize processing conditions in the emerging field of implantation in photovoltaics.

Appendix

A. Parameters of the model

The diffusion model of (1) is termed *Charged Pair* in Sentaurus Process [6]. The full dynamical model *Charged React* leads to equivalent results for the conditions studied in this paper, similarly to the observations of Ref. [13].

Implantations have usually been simulated with the Sentaurus Process Monte Carlo implantation in its default configuration [6]. In order to speed up calculations, for the simulations shown, we used an analytical implantation, using a "+1.4 model". This leads to the same net number of implantation-induced interstitials behind the amorphous-crystalline boundary, as obtained in the Monte Carlo implantation. It therefore leads to the same results for the diffusion profiles.

We use the parameters of the Advanced Calibration of Sentaurus Process [31] as a starting point. In the following, we only specify the parameters that we changed. We used the I clustering model of [14], which turned out to be sufficiently accurate for the conditions discussed in this paper. More sophisticated I clustering (dislocation loop) models [38] yielded almost equivalent results, but required more computational time. An extended discussion of the following parameters can be found in Ref. [38].

The changed diffusion coefficients read $D_{\mathrm{P}^+I^-} = 8.25{\cdot}10^1 \cdot e^{-4.1\,\mathrm{eV}/kT}\,\mathrm{cm}^{-2}/\mathrm{s}$, $D_{\mathrm{P}^+I^0} = 7.80 \cdot 10^1 \cdot e^{-4.0\,\mathrm{eV}/kT}\,\mathrm{cm}^{-2}/\mathrm{s}$ and $D_{\mathrm{P}^+V^=} = 1.83 \cdot 10^{-5} \cdot e^{-2.9\,\mathrm{eV}/kT}\,\mathrm{cm}^{-2}/\mathrm{s}$. The less relevant diffusivities of $D_{\mathrm{P}^+V^-}$ and $D_{\mathrm{P}^+V^0}$ are left unchanged. We furthermore change one pairing rate: $k_{\mathrm{P}^+V^=} = 2.1{\cdot}10^{-26} \cdot e^{1.0\,\mathrm{eV}/kT}\,\mathrm{cm}^2$.

The solid solubility used to solve the diffusion model is set to $2.0 \cdot 10^{21} \cdot e^{-0.1\,\mathrm{eV}/kT}\,\mathrm{cm}^{-3}$ while the solid solubility used to evaluate the simulated data, e.g. for obtaining R_s, is taken as $0.51 \cdot 10^{22} \cdot e^{-0.3\,\mathrm{eV}/kT}\,\mathrm{cm}^{-3}$.[1]

Concerning interface segregation: The emission rate is set to $k_e = 1.04 \cdot 10^{-9} \cdot e^{-3.4\,\mathrm{eV}/kT}\,\mathrm{cm}^3/\mathrm{s}$ for $T < 850\,^\circ\mathrm{C}$ and $k_e = 1.66{\cdot}10^{-11} \cdot e^{-3\,\mathrm{eV}/kT}\,\mathrm{cm}^3/\mathrm{s}$ for $T \geq 850\,^\circ\mathrm{C}$. The trapping rate is set to $k_t = 2.1 \cdot 10^{-29} \cdot e^{-0.7\,\mathrm{eV}/kT}\,\mathrm{cm}^3/\mathrm{s}$. The dissolution rate for an auxiliary clustering reaction $\mathrm{P} \leftrightarrow \mathrm{P}_2$ in the interface, defined in [31], is set to $k_{\mathrm{dis}} = 1.2 \cdot 10^{28} \cdot e^{-3\,\mathrm{eV}/kT}\,\mathrm{cm}^{-2}$.

While the preceding parameters are a general calibration that correctly describes very broad experimental conditions [38], the high precision shown in Figs. 5 and 6, is related to a particular recalibration, for which we changed two diffusivities: $D_{\mathrm{P}^+I^-} = 1.07 \cdot 10^2 \cdot e^{-4.1\,\mathrm{eV}/kT}\,\mathrm{cm}^{-2}/\mathrm{s}$ for $T < 900\,^\circ\mathrm{C}$ and $D_{\mathrm{P}^+I^-} = 4.05 \cdot 10^4 \cdot e^{-4.7\,\mathrm{eV}/kT}\,\mathrm{cm}^{-2}/\mathrm{s}$ for $T \geq 900\,^\circ\mathrm{C}$. $D_{\mathrm{P}^+V^=} = 2.42 \cdot 10^1 \cdot e^{-4\,\mathrm{eV}/kT}\,\mathrm{cm}^{-2}/\mathrm{s}$.

To obtain high precision also for the $4.5{\cdot}10^{15}\,\mathrm{cm}^{-2}$ dose simulation in Fig. 5, we again changed these two diffusivities: $D_{\mathrm{P}^+I^-} = 8.25 \cdot 10^1 \cdot e^{-4.1\,\mathrm{eV}/kT}\,\mathrm{cm}^{-2}/\mathrm{s}$ for $T < 900\,^\circ\mathrm{C}$ and $3.12 \cdot 10^4 \cdot e^{-4.7\,\mathrm{eV}/kT}\,\mathrm{cm}^{-2}/\mathrm{s}$ for $T \geq 900\,^\circ\mathrm{C}$. $D_{\mathrm{P}^+V^=} = 9.59 \cdot 10^{-4} \cdot e^{-3.3\,\mathrm{eV}/kT}\,\mathrm{cm}^{-2}/\mathrm{s}$.

[1]The justification and explanation of this difference is discussed at length in Sec. III. The *activation model* discussed there is called *solid* in Sentaurus Process [6], which is not the default of the Advanced Calibration.

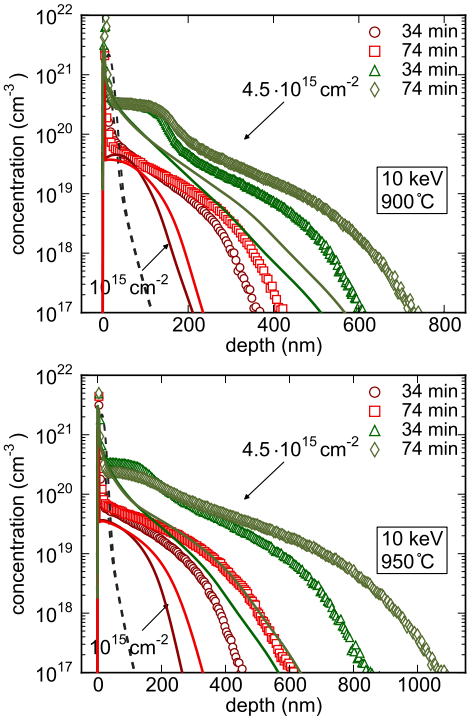

Fig. 9. P concentration profiles for annealing of implanted Phosphorus at 10 keV and doses of $1{\cdot}10^{15}\,\mathrm{cm}^{-2}$ and $4.5{\cdot}10^{15}\,\mathrm{cm}^{-2}$. Symbols depict experimental results from Bosch Solar Energy, lines simulation results. The annealing temperatures and times are given in the panels. Heating and cooling ramps proceed at 10 K/min, starting at 600 °C. The interface to the oxide is at 0 μm. Simulations were performed using [31]. Sentaurus Monte Carlo implantation was used with its default options.

B. Results with Sentaurus Process Advanced Calibration

In Fig. 9, we show the predicition of a state-of-the-arte diffusion model [31] for the typical solar cell relevant experiments we studied. We note that the model of Ref. [31] is mainly adapted to rapid thermal annealing conditions. To describe the latter predictively was not the main focus of the present work. However, several comparisons of the current model for much shorter annealing times can be found in the dissertation of Wolf [38].

REFERENCES

[1] T. Böscke, D. Kania, C. Schollhorn, D. Stichtenoth, A. Helbig, P. Sadler, M. Braun, M. Dupke, M. Weis, A. Grohe, J. Lossen, and H.-J. Krokoszinski, "Fully ion implanted and coactivated industrial n-type cells with 20.5% efficiency," *Photovoltaics, IEEE Journal of*, vol. 4, no. 1, pp. 48–51, Jan 2014. http://dx.doi.org/10.1109/JPHOTOV.2013.2287760

[2] A. Lanterne, S. Gall, Y. Veschetti, R. Cabal, M. Coig, F. Milsi, and A. Tauzin, "High efficiency fully implanted and co-annealed bifacial n-type solar cells," *Energy Procedia*, vol. 38, no. 0, pp. 283 – 288, 2013, proceedings of the 3rd International Conference on Crystalline Silicon Photovoltaics (SiliconPV 2013). http://dx.doi.org/http://dx.doi.org/10.1016/j.egypro.2013.07.279

[3] F. A. Wolf, A. Martinez-Limia, D. Stichtenoth, and P. Pichler, "Modeling the annealing of dislocation loops in implanted c-si solar cells," *Photovoltaics, IEEE Journal of*, vol. 4, no. 3, pp. 851–858, May 2014. http://dx.doi.org/10.1109/JPHOTOV.2014.2312103

[4] J. Krügener, R. Peibst, F. A. Wolf, E. Bugiel, T. Ohrdes, F. Kiefer, C. Schöllhorn, A. Grohe, R. Brendel, and H. J. Osten, "Electrical and structural analysis of crystal defects after high-temperature rapid thermal annealing of highly boron ion-implanted emitters," *accepted by the IEEE Journal of Photovoltaics*, 2014.

[5] P. Pichler, *Intrinsic Point Defects, Impurities, and Their Diffusion in Silicon*, 1st ed. Vienna: Springer, 2004.

[6] SP, *Sentaurus Process User Guide, Version G-2012.06*, 2012. http://www.synopsys.com/Tools/TCAD/Pages/default.aspx

[7] F. A. Wolf, A. Martinez-Limia, and P. Pichler, "A comprehensive model for the diffusion of boron in silicon in presence of fluorine," *Solid-State Electronics*, vol. 87, no. 0, pp. 4–10, 2013. http://dx.doi.org/http://dx.doi.org/10.1016/j.sse.2013.04.027

[8] R. Chen, H. Wagner, A. Dastgheib-Shirazi, M. Kessler, Z. Zhu, P. P. Altermatt, and S. T. Dunham, "Understanding coupled oxide growth and phosphorus diffusion in $POCl_3$ deposition for control of phosphorus emitter diffusion," in *Photovoltaic Specialists Conference (PVSC), 2012 38th IEEE*, 2012, pp. 000 213–000 216. http://dx.doi.org/10.1109/PVSC.2012.6317603

[9] A. Bentzen, A. Holt, J. S. Christensen, and B. G. Svensson, "High concentration in-diffusion of phosphorus in Si from a spray-on source," *Journal of Applied Physics*, vol. 99, no. 6, p. 064502, 2006. http://dx.doi.org/10.1063/1.2179197

[10] A. Bentzen, "Phosphorus diffusion and gettering in silicon solar cells," *PhD thesis (University of Oslo)*, 2006. http://www.ife.no/en/publications/2006/ensys/publication.2007-08-16.4501345468

[11] A. Florakis, T. Janssens, N. Posthuma, J. Delmotte, B. Douhard, J. Poortmans, and W. Vandervorst, "Simulation of the phosphorus profiles in a c-Si solar cell fabricated using $POCl_3$ diffusion or ion implantation and annealing," in *Proceedings of the 3rd International Conference on Crystalline Silicon Photovoltaics (SiliconPV 2013)*, ser. Energy Procedia, R. Brendel, A. Aberle, A. Cuevas, S. Glunz, G. Hahn, J. Poortmans, R. Sinton, and A. Weeber, Eds., vol. 38, 2013, pp. 263–269. http://dx.doi.org/10.1016/j.egypro.2013.07.276

[12] A. Florakis, T. Janssens, J. Poortmans, and W. Vandervorst, "Process modeling for doped regions formation on high efficiency crystalline silicon solar cells," *Journal of Computational Electronics*, vol. 13, no. 1, pp. 95–107, 2014. http://dx.doi.org/10.1007/s10825-013-0487-2

[13] S. T. Dunham, "A quantitative model for the coupled diffusion of phosphorus and point defects in silicon," *Journal of The Electrochemical Society*, vol. 139, no. 9, pp. 2628–2636, 1992. http://dx.doi.org/10.1149/1.2221276

[14] C. S. Rafferty, G. H. Gilmer, M. Jaraiz, D. Eaglesham,

and H.-J. Gossmann, "Simulation of cluster evaporation and transient enhanced diffusion in silicon," *Applied Physics Letters*, vol. 68, no. 17, pp. 2395–2397, 1996. http://dx.doi.org/10.1063/1.116145

[15] P. M. Fahey, P. B. Griffin, and J. D. Plummer, "Point defects and dopant diffusion in silicon," *Rev. Mod. Phys.*, vol. 61, pp. 289–384, Apr 1989. http://dx.doi.org/10.1103/RevModPhys.61.289

[16] W. Shockley and J. T. Last, "Statistics of the charge distribution for a localized flaw in a semiconductor," *Phys. Rev.*, vol. 107, pp. 392–396, Jul 1957. http://dx.doi.org/10.1103/PhysRev.107.392

[17] K. Lehovec and A. Slobodskoy, "Diffusion of charged particles into a semiconductor under consideration of the built-in field," *Solid-State Electronics*, vol. 3, no. 1, pp. 45–50, 1961. http://dx.doi.org/10.1016/0038-1101(61)90079-X

[18] H. Bracht, N. A. Stolwijk, and H. Mehrer, "Properties of intrinsic point defects in silicon determined by zinc diffusion experiments under nonequilibrium conditions," *Phys. Rev. B*, vol. 52, pp. 16 542–16 560, Dec 1995. http://dx.doi.org/10.1103/PhysRevB.52.16542

[19] J. S. Christensen, H. H. Radamson, A. Y. Kuznetsov, and B. G. Svensson, "Phosphorus and boron diffusion in silicon under equilibrium conditions," *Applied Physics Letters*, vol. 82, no. 14, pp. 2254–2256, 2003. http://dx.doi.org/10.1063/1.1566464

[20] J. S. Christensen, A. Y. Kuznetsov, H. H. Radamson, and B. G. Svensson, "Phosphorus diffusion in silicon; influence of annealing conditions," *MRS Proceedings*, vol. 669, J3.9, 2001. http://dx.doi.org/10.1557/PROC-669-J3.9

[21] N. R. Zangenberg, J. Fage-Pedersen, J. L. Hansen, and A. N. Larsen, "Boron and phosphorus diffusion in strained and relaxed Si and SiGe," *Journal of Applied Physics*, vol. 94, no. 6, pp. 3883–3890, 2003. http://dx.doi.org/10.1063/1.1602564

[22] Y. M. Haddara, B. T. Folmer, M. E. Law, and T. Buyuklimanli, "Accurate measurements of the intrinsic diffusivities of boron and phosphorus in silicon," *Applied Physics Letters*, vol. 77, no. 13, pp. 1976–1978, 2000. http://dx.doi.org/10.1063/1.1313248

[23] M. Uematsu, "Simulation of boron, phosphorus, and arsenic diffusion in silicon based on an integrated diffusion model, and the anomalous phosphorus diffusion mechanism," *Journal of Applied Physics*, vol. 82, no. 5, pp. 2228–2246, 1997. http://dx.doi.org/10.1063/1.366030

[24] R. B. Fair and J. C. C. Tsai, "A quantitative model for the diffusion of phosphorus in silicon and the emitter dip effect," *Journal of The Electrochemical Society*, vol. 124, p. 1107, 1977. http://dx.doi.org/10.1149/1.2133492

[25] E. Tannenbaum, "Detailed analysis of thin phosphorus-diffused layers in *p*-type silicon," *Solid-State Electronics*, vol. 2, no. 2-3, pp. 123–132, 1961. http://dx.doi.org/10.1016/0038-1101(61)90029-6

[26] N. K. Abrikosov, V. M. Glazov, and L. Chen-yüan, "Individual and joint solubilities of aluminium and phosphorus in germanium and silicon," *Russian Journal of Inorganic Chemistry*, vol. 7, pp. 429–431, 1962.

[27] S. Solmi, A. Parisini, R. Angelucci, A. Armigliato, D. Nobili, and L. Moro, "Dopant and carrier concentration in Si in equilibrium with monoclinic SiP precipitates," *Phys. Rev. B*, vol. 53, pp. 7836–7841, Mar 1996. http://dx.doi.org/10.1103/PhysRevB.53.7836

[28] A. Carabelas, D. Nobili, and S. Solmi, "Grain boundary segregation in silicon heavily doped with phosphorus and arsenic," *Journal de Physique*, vol. 43, no. 10, pp. 187–192, 1982.

[29] J. Götzlich, P. Tsien, and H. Ryssel, "Relaxation behavior of metastable As and P concentrations in Si after pulsed and CW laser annealing," *MRS Proceedings*, vol. 23, 235, 1983. http://dx.doi.org/10.1557/PROC-23-235

[30] H. R. Soleimani, "An investigation of phosphorus transient diffusion in silicon below the solid solubility limit and at a low implant energy," *Journal of The Electrochemical Society*, vol. 141, no. 8, pp. 2182–2188, 1994. http://dx.doi.org/10.1149/1.2055083

[31] SPAC, *Advanced Calibration for Sentaurus Process User Guide, Version G-2012.06*, 2012. http://www.synopsys.com/Tools/TCAD/Pages/default.aspx

[32] P. B. Griffin, S. W. Crowder, and J. M. Knight, "Dose loss in phosphorus implants due to transient diffusion and interface segregation," *Applied Physics Letters*, vol. 67, no. 4, pp. 482–484, 1995. http://dx.doi.org/10.1063/1.114543

[33] F. Lau, L. Mader, C. Mazure, C. Werner, and M. Orlowski, "A model for phosphorus segregation at the silicon-silicon dioxide interface," *Applied Physics A: Materials Science and Processing*, vol. 49, pp. 671–675, 1989, 10.1007/BF00616992. http://dx.doi.org/10.1007/BF00616992

[34] M. Orlowski, "New model for dopant redistribution at interfaces," *Applied Physics Letters*, vol. 55, no. 17, pp. 1762–1764, 1989. http://dx.doi.org/10.1063/1.102210

[35] Y.-S. Oh and D. Ward, "A calibrated model for trapping of implanted dopants at material interface during thermal annealing," *International Electron Devices Meeting (IEDM)*, pp. 509 –512, dec 1998. http://dx.doi.org/10.1109/IEDM.1998.746409

[36] M. G. Kang, J.-H. Lee, H. Boo, S. J. Tark, H. C. Hwang, W. J. Hwang, H. O. Kang, and D. Kim, "Effects of annealing on ion-implanted Si for interdigitated back contact solar cell," *Current Applied Physics*, vol. 12, no. 6, pp. 1615–1618, 2012. http://dx.doi.org/10.1016/j.cap.2012.05.035

[37] M. Chun, B. Adibi, H. Hieslmair, and L. Mandrell, "Using solid phase epitaxial re-growth for ion implantation in solar cell fabrications," *EU PVSEC Proceedings*, vol. 26, pp. 1293–1296, 2011. http://dx.doi.org/10.4229/26thEUPVSEC2011-2BV.1.25

[38] F. A. Wolf, "Modeling of annealing processes for ion-implanted single-crystalline silicon solar cells," Ph.D. dissertation, University of Erlangen-Nuremberg, 2014. http://nbn-resolving.de/urn:nbn:de:bvb:29-opus4-49068

F. Alexander Wolf obtained a M. Sc. in Physics in 2011 from the University of Augsburg. At the time of this work, he was a PhD student at Bosch Corporate Research, Gerlingen, Germany. He now is with the Ludwig-Maximilians-Universität (LMU), Munich.

Alberto Martinez-Limia obtained his diploma in Nuclear Physics in 1994 from the Institute of Nuclear Sciences and Technology of Havana and his PhD in 2002 from the Institute of Theoretical Chemistry of the University of Erlangen-Nuremberg. Later he worked in several academic and scientific organizations: the University of South Carolina, the University of Chemnitz and the Fraunhofer Institute IISB in Erlangen. He investigated topics related to material modeling and process simulation. In October 2008 he joined the Robert Bosch GmbH as a Research and Development scientist.

Daniela Grote studied physics at the Universities of Marburg and Freiburg, Germany. She received her diploma degree in physics in 2004 from the University of Freiburg. In 2010 she obtained her Dr. rer. nat. from the University of Konstanz. Both diploma thesis and dissertation focus on different aspects of the characterization and simulation of silicon solar cells and were realized at the Fraunhofer Institute for Solar Energy Systems ISE, Freiburg, Germany. In 2010 Daniela Grote joined the Bosch Solar Energy AG, Arnstadt, Germany, and is now with the SolarWorld Industries Thüringen GmbH, Arnstadt, Germany.

Daniel Stichtenoth studied physics at the University of Göttingen, Germany and Uppsala, Sweden. He received his diploma degree in physics in 2005 and his Dr. rer nat in 2008 from the University of Göttingen, Germany. Since 2009 he is with BOSCH Solar Energy AG, Arnstadt, Germany and works in the field of silicon solar cell development. His main focus is on the interaction of silicon with high-efficiency silicon solar cell processes.

Peter Pichler obtained the Dip.-Ing. degree in Electrical Engineering in 1982 and the Dr. techn. degree 1985 both from the Technical University of Vienna. Since 1986 he has been Group Manager at Fraunhofer IISB, responsible now for the doping and device simulation activities. In 2004 he obtained the venia legendis from the University of Erlangen-Nuremberg. Dr. Pichler contributed to various European projects and coordinated the EC projects RAPID, FRENDTECH, ATOMICS and ATEMOX on diffusion and activation phenomena in silicon and silicon-based materials, as well as on the modeling of leakage currents and technologies for low-leakage ultrashallow junctions. He is the author or coauthor of some 120 publications in international journals and conference proceedings, and author of the book “Intrinsic Point Defects, Impurities, and Their Diffusion in Silicon” published by Springer Wien-New York.